Designed Multifunctional Spider Silk Enabled by Genetically Encoded Click Chemistry

Jiang, Bojing; Tan, Sin Yen; Fang, Shiyu; Feng, Xiaohan; Park, Byung Min; Fok, Hong Kiu Francis; Yang, Zhongguang; Wang, Ri; Kou, Songzi; Wu, Angela Ruohao

DOI
10.1002/adfm.202304143

Publication date
2023

Document Version
Final published version

Published in
Advanced Functional Materials

ADVANCED FUNCTIONAL MATERIALS
www.afm-journal.de

Designed Multifunctional Spider Silk Enabled by Genetically Encoded Click Chemistry

Bojing Jiang, Sin Yen Tan, Shiyu Fang, Xiaohan Feng, Byung Min Park, Hong Kiu Francis Fok, Zhongguang Yang, Ri Wang, Songzi Kou, Angela Ruohao Wu, and Fei Sun**

Spider silk is recognized for its exceptional mechanical properties and biocompatibility, making it a versatile platform for developing functional materials. In this study, a modular functionalization strategy for recombinant spider silk is presented using SpyTag/SpyCatcher chemistry, a prototype of genetically encoded click chemistry. The approach involves AlphaFold2-aided design of SpyTagged spider silk coupled with bacterial expression and biomimetic spinning, enabling the decoration of silk with various SpyCatcher-fusion motifs, such as fluorescent proteins, enzymes, and cell-binding ligands. The silk threads can be coated with a silica layer using silicatein, an enzyme for silicification, resulting in a hybrid inorganic–organic 1D material. The threads installed with RGD or laminin cell-binding ligands lead to enhanced endothelial cell attachment and proliferation. These findings demonstrate a straightforward yet powerful approach to 1D protein materials.

1. Introduction

Spider silk is a biopolymer that exhibits exceptional tensile strength, extensibility, biocompatibility, biodegradability, and hypoallergenic properties.[1] It has been extensively researched for various applications, including biosensors,[2] surgical sutures,[1b,3] textiles,[4] optical waveguiding,[5] and nerve regeneration.[6] However, large-scale production of spider silk through farming is impractical due to cannibalistic behavior of spiders and the low yield. An alternative approach is to produce recombinant spider silk protein (spidroin) in heterologous hosts using genetic engineering.[7] Highly soluble spidroins have been produced with a high yield using *Escherichia coli* ,[8] which, followed by biomimetic spinning, has resulted in fibers with high tensile strength and extensibility, comparable to the mechanical properties of natural spider silk.[9]

Despite their exceptional mechanical properties and potential for biomedical applications, it remains challenging to biochemically functionalize 1D materials for specific biomedical purposes.[10] This is due to the delicate and sensitive nature of these protein fibers, which require gentle methods to preserve their mechanical properties while effectively modifying their surface under mild conditions. In recent years, genetically encoded click chemistries (GECCs), which enable specific and efficient covalent bonding between protein components, have become valuable tools for constructing advanced protein architectures and bioactive materials.[11] For instance, Spy chemistry from the GECC toolbox, which comprises a peptide/protein pair that spontaneously forms a Lys–Asp isopeptide bond, enables covalent conjugation of modular protein components onto sophisticated materials without chemical modification.[12] It provides selective and efficient ligation between protein molecules, at their N-, C-terminal, or even middle regions, distinguishing it from other methods such as sortase ligation and split intein that mediate protein ligations invariably

B. Jiang, S. Y. Tan, S. Fang, X. Feng, B. M. Park, H. K. F. Fok, Z. Yang, R. Wang, A. R. Wu, F. Sun
Department of Chemical and Biological Engineering
The Hong Kong University of Science and Technology
Clear Water Bay, Kowloon, Hong Kong SAR China
E-mail: angelawu@ust.hk; kefsun@ust.hk

B. Jiang
Department of Energy, Environmental and Chemical Engineering
Washington University in St. Louis
Saint Louis, MO 63130, USA

B. M. Park
Department of Imaging Physics
Delft University of Technology
Delft 2628 CD, The Netherlands

Z. Yang
SPES Tech Limited
New Territories, Hong Kong SAR China

S. Kou, F. Sun
Greater Bay Biomedical InnoCenter
Shenzhen Bay Laboratory
Shenzhen 518036, China

A. R. Wu
Division of Life Science
The Hong Kong University of Science and Technology
Clear Water Bay, Kowloon, Hong Kong SAR China

The ORCID identification number(s) for the author(s) of this article can be found under https://doi.org/10.1002/adfm.202304143

DOI: 10.1002/adfm.202304143

from N- to C-terminal.[13] Given its proven robustness and versatility, Spy chemistry offers a simple and modular approach to functionalize recombinant spider silk.

In this study, we created SpyTag-presenting spider silk through a combination of *E. coli* expression and biomimetic spinning, which allowed for its modular functionalization using Spy chemistry for 1D biomineralization and cell culturing. These clickable spider silk fibers possess the potential for controlled biological patterning, owing to their capacity to organize bioactive ligands or even living cells in a 1D manner.

2. Results and Discussion

2.1. Protein Design and Construction

Our objective was to produce modular, multi-functional 1D biomaterials using GECC. To this end, we used the SpyTag/SpyCatcher pair, referred as "A" and "B", respectively, and a chimeric mini-spidroin as a model system to generate 1D biomaterials.[8] The chimeric spidroin consisted of three domains, including the middle two repetitive Gly- and Ala-rich units (2R) – which provide rigidity and strength – flanked by the N-terminal domain (NTD) of MaSp1 derived from *Euprosthenops australis* and the C-terminal domain (CTD) of MiSp from *Araneus ventricosus*. The more conserved NTD and CTD in spidroin, which are highly soluble and pH-sensitive, are responsible for spidroin storage in the gland and the initiation of the fiber assembly process. The CTD adopts a parallel dimeric structure in both the dope and fiber states.[14] In contrast, the NTD is monomeric in the dope,[15] and turns into stable antiparallel homodimers in the fiber states under the influence of shear force and low pH.[14a,16] We fused SpyTag to the CTD of minispidroin, while introducing a flexible linker (GGGGSGGGGSGGGGS) to avoid steric hindrance of functional protein domains (**Figure 1**). According to the structural predications made by AlphaFold2[17] and AlphaFold2-multimer_v3[18] under ColabFold[19] (Table S5, Supporting Information), attaching SpyTag to the CTD of spidroin, instead of its NTD, may also help prevent the interference between SpyTag and spidroin;[9] SpyTag, when fused at the CTD, is spatially apart from spidroin, which is not the case when placed at the NTD.

A. R. Wu
Hong Kong Branch of Guangdong Southern Marine Science and Engineering Laboratory (Guangzhou)
Hong Kong University of Science and Technology
Clear Water Bay, Kowloon, Hong Kong SAR China
A. R. Wu
State Key Laboratory of Molecular Neuroscience
The Hong Kong University of Science and Technology
Clear Water Bay, Kowloon, Hong Kong SAR China
F. Sun
Biomedical Research Institute
Shenzhen-Peking University–The Hong Kong University of Science and Technology Medical Center
Shenzhen 518036, China
F. Sun
HKUST Shenzhen Research Institute
Shenzhen 518057, China

To test the feasibility of immobilizing proteins onto the surface of silk via Spy chemistry, we generated a series of recombinant fluorescent proteins, including SpyTag-ELP-EGFP-ELP-SpyTag (AGFPA; AGA), SpyCatcher-ELP-EGFP-ELP-SpyCatcher (BGFPB; BGB), SpyCatcher-ELP-CFP-ELP-SpyCatcher (BCFPB), SpyCatcher-cpYFP-SpyCatcher (BcpYFPB), and SpyCatcher-ELP-mCherry-ELP-SpyCatcher (BmCherryB). We also aimed to develop a 1D inorganic–organic hybrid material through biocatalysis. Silicatein, a natural biomineralizing enzyme, is well-known for its ability to catalyze the polymerization of silica.[20] However, its aggregation, poor solubility, and low expression yield have limited its use. To overcome these issues, we genetically fused silicatein with two elastin-like polypeptide (ELP) domains to create the SpyCatcher-ELP-Silicatein α1-ELP-SpyCatcher (BSaTB) construct. The ELPs, which consist of repeating pentapeptides $(VPGXG)_{15}$, where X represents either Val or Glu at a 4:1 ratio, are noted for the high solubility and high-yield expression in *E. coli*.[12] The composition of these ELPs leads to a lower critical solution temperature (LCST) of 45–60 °C,[12] which is above the temperatures used in most experiments in this study.

Another objective was to examine the feasibility of using engineered spider silk as a 1D carrier of bioactive ligands and living cells to promote the formation of vascular network – a process crucial for advanced tissue engineering. To this end, we created the constructs, including SpyCatcher-ELP-2GRGDSP-ELP-SpyCatcher (B2RGDB) and SpyCatcher-ELP-Laminin α1 MMPQK-ELP-SpyCatcher (BLMB), which harbor the cell-binding fibronectin-derived peptide (GRGDSP), laminin-derived peptide α1, matrix metalloproteinase-1 (MMP-1) cleavage sequence, and vascular endothelial growth factor (VEGF)-mimetic peptide (QK), respectively.[21] These motifs have previously been shown to promote the growth and proliferation of endothelial cells and subsequent vascular network formation, which we anticipate would also endow the decorated spider silk with similar capabilities.

2.2. Production of SpyTagged Spider Silk

The spidroin-SpyTag (S-A) protein was produced in *E. coli* and purified using Ni-NTA affinity chromatography. Consistent with the previous findings,[22] the purified spidroin was sensitive to the ionic strength of solvents. The protein solutions at high concentration (7 mg mL^{-1}) were clear in the presence of monovalent Cl^-, and became turbid in the presence of trivalent PO_4^{3-} (Figure S5, Supporting Information), the latter of which indicates phosphate-induced liquid-liquid phase separation caused by the transition of spidroin into fibril structures.[23] For this reason, we avoided phosphate-buffered solvents in the ensuing spinning process to produce silk fibers (Figure S3b, Supporting Information).

By mimicking the spider's spinning process in the major ampullate glands,[9] we were able to achieve the scale-up production of recombinant spider silk comprising spidroin–SpyTag (S-A) (Figure S3c, Supporting Information). To facilitate this biomimetic spinning, we assembled a microinjection syringe pump with a protein spinning dope-loaded syringe and a 34 G stainless steel blunt-tip needle, which extrudes continuous silk threads into an acidic coagulation bath (pH 5.0) (Figure S1, Supporting Information). The pH of 5 was selected as it has

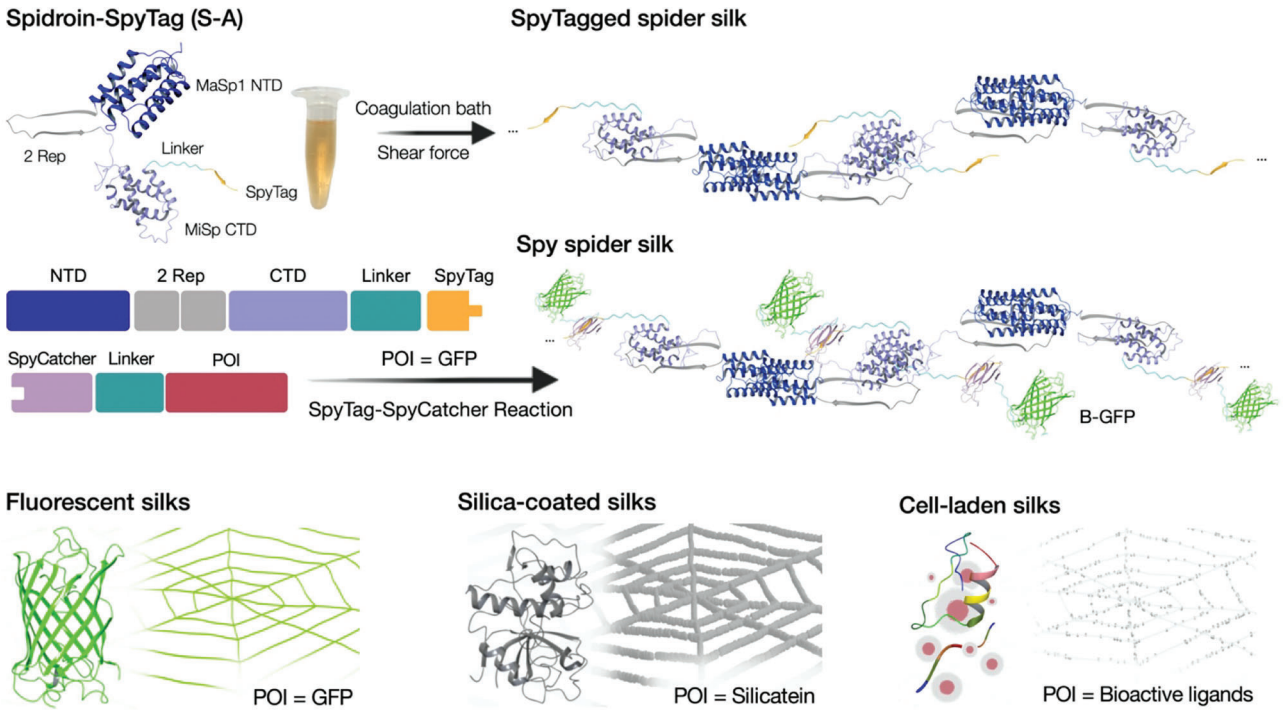

Figure 1. Schematic showing the creation of multifunctional Spy spider silk via genetically encoded click chemistry. Recombinant spider silk fused with SpyTag can be decorated with a variety of SpyCatcher-fusion proteins of interest (POI), ranging from fluorescent proteins, enzymes (e.g., silicatein), to bioactive ligands (e.g., RGD- and/or laminin-cell binding motifs).

previously been shown to be suitable for inducing the transition of soluble spidroins into silk fibers.[8,24] The underwater roller reeling process was designed to avoid the non-uniformity of size induced by stretching, and post-spin incubation in the coagulation bath was intended to further enhance the mechanical and wet-resistant properties of the silk, which is associated with an increase in β-sheet content.[25] The entire spinning device comprises standardized industrial products, which simplifies scale-up compared to microfluidic devices and pulled-glass capillaries.

The silk threads obtained from spinning exhibited a smooth surface and cross-sections, as revealed by polarized optical microscopy (Figure 3a) and scanning electron microscopy

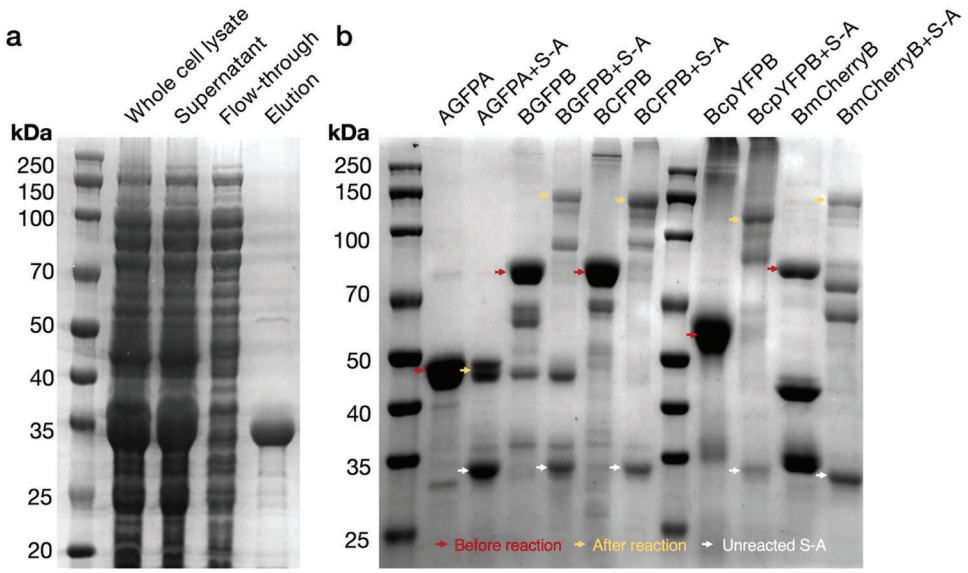

Figure 2. Bacterial expression of spidroin-SpyTag (S–A) and its reactions with SpyCatcher-fusion proteins. a) SDS-PAGE analyses of S-A expressed by *E. coli* and b) its reactions with SpyCatcher-fusion proteins.

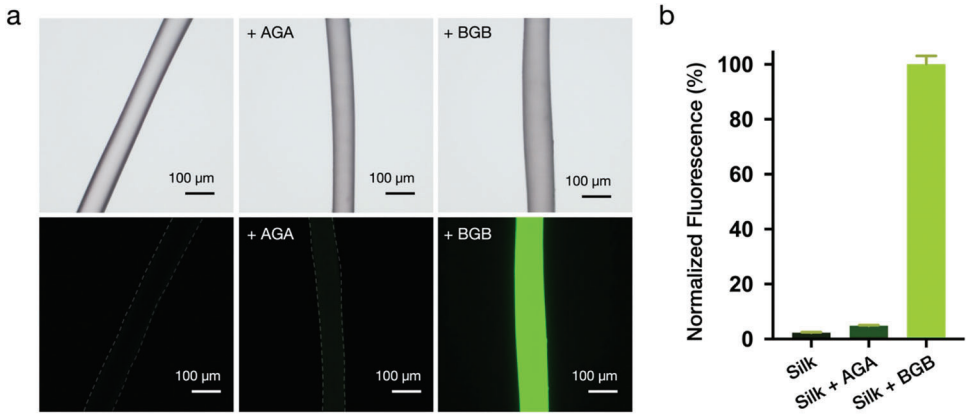

Figure 3. Spy chemistry is essential for the efficient decoration of spider silk with proteins. a) Reactions of SpyTagged spider silk with SpyTag-ELP-GFP-ELP-SpyTag (AGA) and SpyCatcher-ELP-GFP-ELP-SpyCatcher (BGB). The silk was immersed in the corresponding protein solution or blank PBS overnight, followed by intense wash with ddH_2O, PBST, and ddH_2O in order. b) Quantification of fluorescence intensity of GFP-decorated silk using ImageJ. Data are presented as means ± SD (number of silk threads, $n = 3$).

(Figure 5a). The silk was found to be highly stable even under extreme conditions. The silk threads remained intact after immersion in 0.1 M NaOH or treatment with 2.5% trypsin at 37 °C overnight. Under the acidic condition (0.1 M HCl), the silk threads turned translucent but remained intact. In contrast, these silk threads readily dissolved in organic acids such as formic acid and under denaturing conditions such as 8 M urea, which could be attributed to protein unfolding under these conditions (Figure S4, Supporting Information).

2.3. Protein Decoration of SpyTagged Spider Silk

According to the SDS-PAGE analyses, the silk precursor, SpyTagged spidroin, can be covalently decorated by SpyCatcher-fusion fluorescent proteins (i.e., BGFPB, BCFPB, BcpYFPB, and BmCherryB), as evidenced by their significant shifts in molecular weight, but not by SpyTag-ELP-EGFP-ELP-SpyTag (AGFPA) (**Figure 2**b). To examine the feasibility of using these SpyCatcher-fusion proteins to directly decorate the resulting SpyTagged spider silk, we treated the materials with these fluorescent proteins in phosphate-buffered saline (PBS, pH 7.4). The silk threads treated with the SpyCatcher-fusion proteins, but not those with AGFPA, exhibited strong fluorescence, which was resistant to intense wash by the Triton X-100 surfactant, as expected for stable conjugation enabled by Spy chemistry (**Figure 3**a,b). It has also proven feasible to incorporate multiple SpyCatcher-fusion fluorescent proteins onto a single silk thread, generating a multicolored protein fiber, which highlights the robustness of Spy chemistry in decorating the recombinant spider silk (**Figure 4**).

2.4. Decoration of Spider Silk with Biomineralizing Enzyme

Silicatein is a silica-polymerizing hydrolase found in marine sponges that catalyzes the hydrolysis of silicon compounds, such as tetraethyl orthosilicate (TEOS), and polymerizes the resulting silicic acid into silica under mild physiological conditions.[26] This enzymatic biomineralization process provides a robust approach for modulating the stability and mechanics of protein materials. To achieve this with recombinant spider silk, we cloned and produced the recombinant protein SpyCatcher-ELP-Silicatein α1-ELP-SpyCatcher (BSaTB) using an *E. coli* expression system, in which silicatein α1 (SaT) was derived from *Tethya Aurantium*. After incubating with BSaTB (15 μM) for one day, the silk threads were immersed in a tetraethyl orthosilicate (TEOS) solution (100 mM). The subsequent SEM analysis revealed a rough, coarse surface and cross-section of the silk threads, in contrast to the smooth fibers immediately after spinning (**Figure 5**b), indicating the formation of a silica coating on the silk threads. To further confirm silicification, X-ray photoelectron spectroscopy (XPS) was used. Two additional peaks at electron binding energies (EB) of 103.4 and 154.4 eV, corresponding to Si 2p and Si 2s, respectively, were observed from the silk threads after biomineralization, but not from those before biomineralization (Figure 5c). Peak-fitting analysis showed that the predominant O 1s peak was at EB of 532.5 eV, corresponding to the oxygen in Si–O–Si. Quantitative XPS analyses showed that 23% Si and 55% O (i.e., a molar ratio of ≈1:2.4) were present on the silk surface, further confirming the formation of silica (SiO_2) on the silk surface. Taken together, these results successfully demonstrate the use of silicatein-laden spider silk as a suitable scaffold for creating hybrid inorganic–organic 1D materials.

2.5. Endothelial Cell Attachment and Proliferation Enabled by Bioactive Spider Silk Fibers

Spider dragline silk is a promising biomaterial with exceptional mechanical properties, making it a potential candidate for an artificial extracellular matrix (ECM).[27] We investigated the cytocompatibility of Spy spider silk as a 1D ECM for human umbilical vein endothelial cells (HUVECs), a model cell line widely used in angiogenic biomaterial research. Our aim was to enhance endothelial cell (EC) adhesion and proliferation using silk fibers functionalized with bioactive motifs.

To this end, we created two SpyCatcher-fusion proteins, SpyCatcher-ELP-2GRGDSP-ELP-SpyCatcher (B2RGDB) and SpyCatcher-ELP-Laminin α1 MMPQK-ELP-SpyCatcher (BLMB),

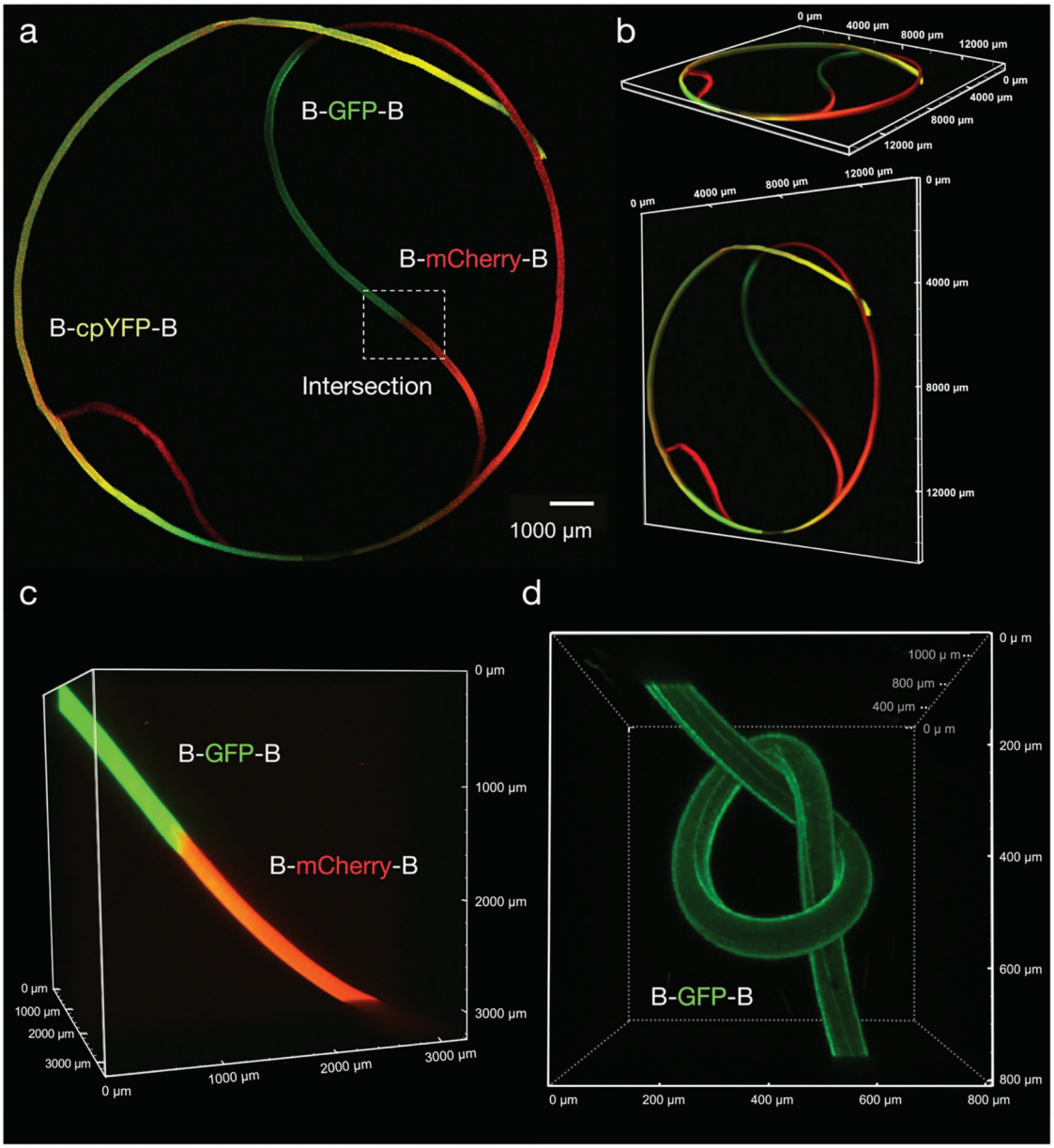

Figure 4. Decoration of spider silk with fluorescent proteins. a,b) a) 2D projection and b) 3D rendering of a S-A silk thread decorated with GFP, cpYFP, and mCherry. c) the intersection indicated in (a) at higher magnification. d) Knotted silk thread after GFP decoration, showing amenability to mechanical deformation.

that possess putative cell binding ligands, Arg-Gly-Asp (RGD) and α1 peptide of laminin, respectively. B2RGDB contains two consecutive RGDs, a motif that is found in many natural ECM proteins, such as fibronectin, and has been widely applied to promote endothelialization on biomaterials.[28] BLMB contains several bioactive motifs including the α1 peptide, a major motif derived from laminin that is known to support the vascularization of EC,[29] and QK, a vascular endothelial growth factor-mimetic peptide.[21c] The matrix-metalloproteinase (MMP) cleavage sequence was also incorporated into B2RGDB and BLMB, which may facilitate vascular remodeling, angiogenesis, proliferation, and survival of endothelial cells.[30]

The silk threads were first reeled onto a steel frame in a loose mesh format (Figure S8, Supporting Information), followed by incubation with the solution of B2RGDB or BLMB. The resulting materials were then tested for their abilities to support EC adhesion and proliferation. Compared with the undecorated ones, the silk threads adorned with the cell-binding motifs exhibited significantly enhanced the EC attachment, viability, and proliferation (**Figure 6**a–e). The cell densities reached up to ≈15 per millimeter of RGD- and laminin-laden silk threads, in contrast to merely one cell per millimeter of undecorated silk (Figure 6b). The presence of the cell-binding ligands on the silk threads significantly increased the long-term cell viability, an attribute crucial for

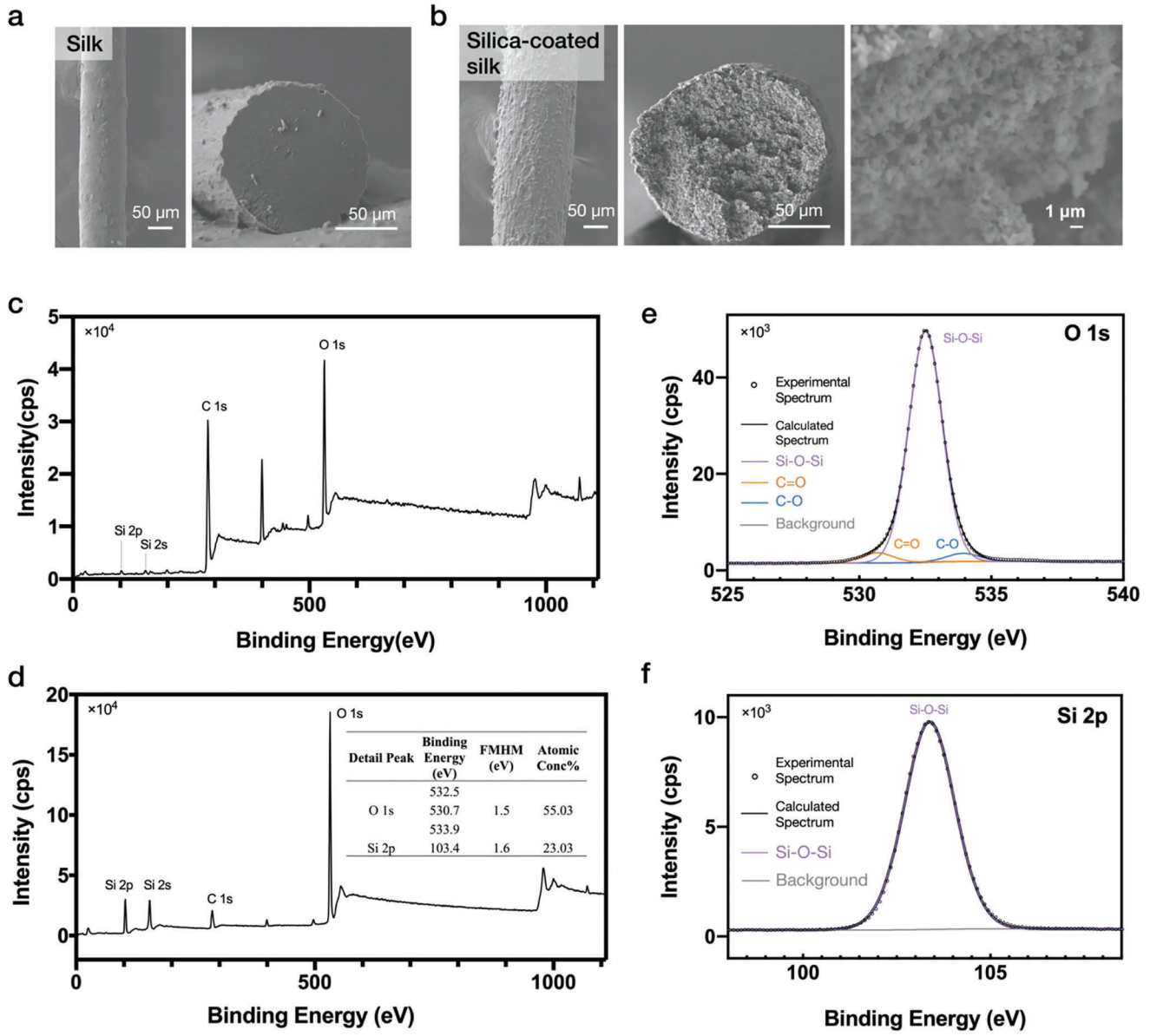

Figure 5. Silica coating of spider silk enabled by silicatein decoration. a,b) SEM images of the top and cross-sectional views of a) S-A silk and b) silica-coated, silicatein-laden S-A silk. c,d) c) XPS analyses of S-A silk and d) silica-coated, silicatein-laden S-A silk. e,f) Zoom-in view of XPS spectra, corresponding to those of e) O 1s and f) Si 2p in (d).

tissue engineering applications; after 6-day culturing, 93 ± 10% and 92 ± 7% of the cells remained viable on the laminin- and RGD-laden surfaces, respectively, while this number for the undecorated stood at 74 ± 11% (Figure 6c). The laminin exerted larger effects on cell behavior than did RGD; after 10-day culturing, the cells covered ≈67%, ≈43%, and ≈23% of the laminin-, RGD-laden, and blank silk surfaces, respectively (Figure 6d). Moreover, the cells on the laminin- and RGD-laden surfaces displayed elongated spindle morphology, in comparison to those on the blank silk that were mostly polygonal or spheric. The larger aspect ratio of those cells observed on the laminin- and RGD-laden surface also indicates a better endothelial function and the potential for endothelialization (Figure 6e). Together, these results demonstrated the importance of the cell-binding motifs such as RGD and laminin for Spy spider silk to become a bioactive and cytocompatible 1D ECM conducive to EC proliferation and alignment. The amenability of these materials to diverse biofunctionalization might help unleash its potential for tissue engineering applications.

Results and DiscussThis study presents a versatile and powerful strategy for the functionalization of recombinant spider silk. The enabling technology, Spy chemistry, allows for incorporation of various motifs including fluorescent proteins, enzymes, and cell-binding ligands onto the silk threads after the spinning process, providing better control and flexibility, compared to genetic

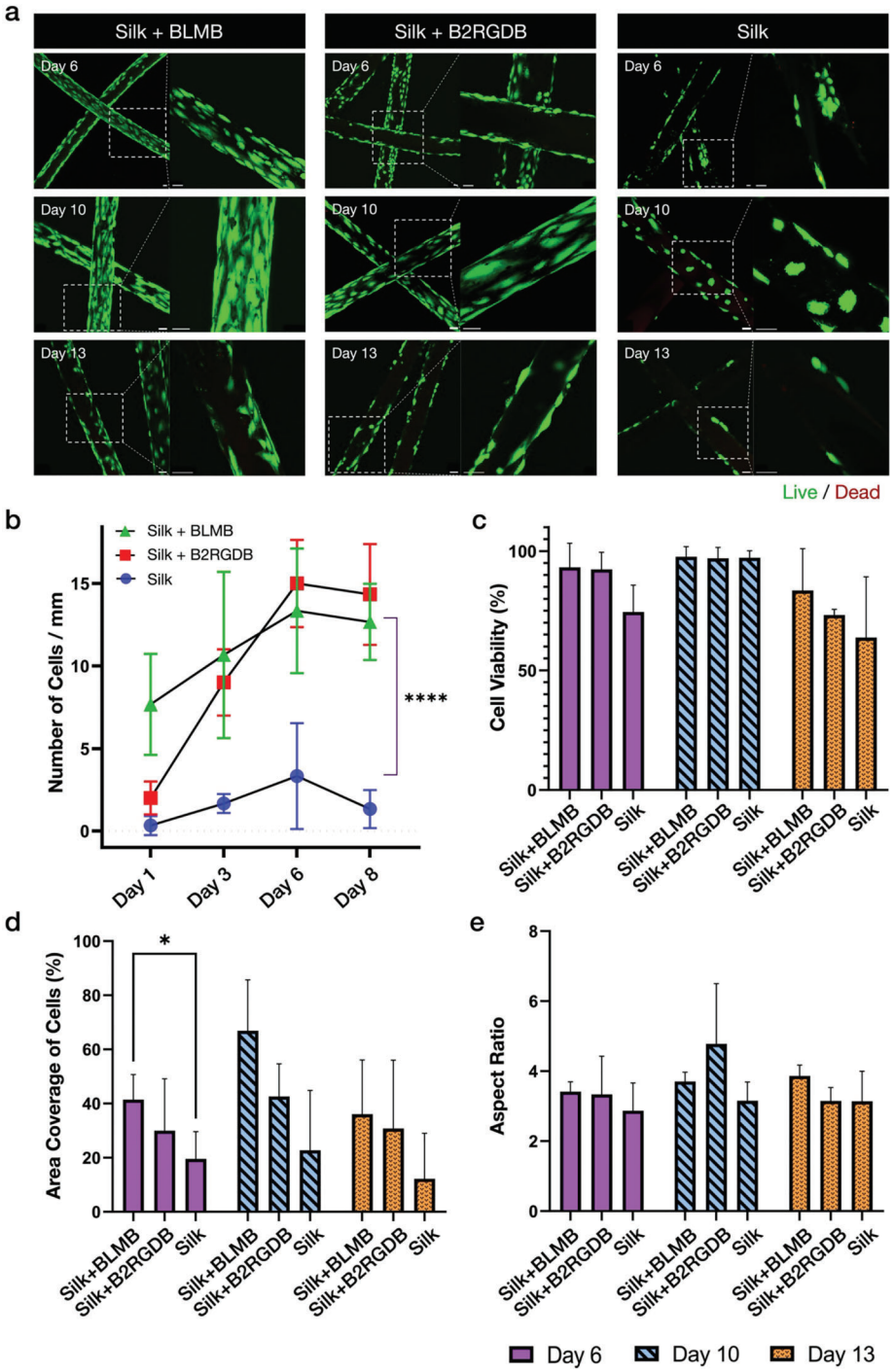

Figure 6. Culturing of endothelial cells on silk decorated with bioactive ligands. a) Representative fluorescence images of Live/Dead stained cells on undecorated silk threads and those decorated by laminin and RGD on days 6, 10, and 13. Scale bar = 50 µm. b) Number of cells per millimeter of silk. c) Quantitative analysis of cell viability on silk. d) Percentage of area covered by cells on the surface of silk. e) Aspect ratio of cells, which is defined as the ratio of cell length to width. Four independent experiments were performed. Data are presented as means ± SD (n = 4). $^{*}p < 0.05$, $^{**}p < 0.01$, $^{***}p < 0.001$.

engineering or other chemical conjugation methods. Though rarely, the efficiency of Spy chemistry may still be contextual, depending on the structural and physicochemical characteristics of functional motifs that are attached. In addition, while the spider silk can be converted to a hybrid inorganic–organic 1D material via biomineralization or a 1D bioactive scaffold conducive to the attachment and proliferation of ECs, further studies are needed to address the remaining challenges, including mechanical tuning, scale-up production, and potential immunogenicity. Overall, this study offers a straightforward yet effective approach to the

development of 1D protein materials, which could have significant implications for tissue engineering applications.

3. Experimental Section

Gene Construction: The construct NTD2RepCTD-SpyTag (S-A) consisted of a N-terminal domain (NTD; EMBL accession no. AM259067EMBL), two repetitive units (2Rep; EMBL accession no. AJ973155) of MaSp1 (*Euprosthenops australis*), a C-terminal domain (CTD; GenBank accession no. JX513956) of MiSp (*Araneus ventricosus*), and a SpyTag domain (A; GenBank accession no. JQ478411) of CnaB2 (*Streptococcus pyogenes*). The fluorescent proteins used in this study included enhanced green fluorescent protein (EGFP; GFP), cyan fluorescent protein (CFP), circularly permuted yellow fluorescent protein (cpYFP), and monomeric red fluorescent protein (mCherry). The mature enzyme (aa113-330) was derived from the silicatein α1 (SaT) domain of *Suberites domuncula* (GenBank accession no. CAI46305). The 2RGD stands for two consecutive fibronectin-derived cell adhesion peptides Gly-Arg-Gly-Asp-Ser-Pro (GRGDSP)[31] linked by two elastin-link peptides (VPGXG). The Laminin α1 MMPQK (LM) is a fusion peptide comprising a laminin α1 peptide (Ac-TFALRGDNP-NH_2),[21c] an optimized matrix metalloproteinase peptide MMP-1 (Ac-VPMS↓MRGG-NH_2),[32] and a vascular endothelial growth factor (VEGF)-mimetic peptide QK (Ac-KLTWQELYQLKYKGI-NH_2).[21d]

The fusion genes, *NdeI-NTD-2Rep-CTD-Linker-SpyTag-XhoI* (S-A) and *NdeI-SpyTag-SacI-cpYFP-BamHI-SpyCatcher-XhoI*, were chemically synthesized by Genewiz Inc., optimized based on *Escherichia coli* codon usage, and inserted into the expression vector pET22b(+) via NdeI and XhoI restriction enzyme sites. To construct pQE80l::*SpyTag-ELP-EGFP-ELP-SpyTag* (*AGFPA*), the *GFP* gene was inserted into pQE80l::*AA*[12] using SacI and SpeI restriction enzyme sites. Similarly, the other constructs, including pQE80l::*SpyCatcher-ELP-GFP-ELP-SpyCatcher* (*BGFPB*), *SpyCatcher-ELP-CFP-ELP-SpyCatcher* (*BCFPB*), *SpyCatcher-ELP-mCherry-ELP-SpyCatcher* (*BmCherryB*), *SpyCatcher-ELP-2GRGDSP-ELP-SpyCatcher* (*B2RGDB*), *SpyCatcher-ELP-Laminin α1 MMPQK-ELP-SpyCatcher* (*BLMB*), and *SpyCatcher-ELP-Silicatein α1-SpyCatcher* (*BSaTB*) were all constructed by inserting the corresponding sequences into pQE80l::*BB*[12] using SacI and SpeI restriction enzyme sites.[33]

For plasmid amplification and molecular cloning, the *E. coli* strain DH5α was utilized. The sequences of all constructs were verified by Sanger sequencing (BGI Hong Kong Ltd.). The Supplementary Information lists the construct information, including that of gene sequences (Table S1, Supporting Information), amino acid sequences (Table S2, Supporting Information), MALDI-TOF mass spectra (Table S3, Supporting Information), and bacterial strains and plasmids (Table S4, Supporting Information) used in this study.

Recombinant Protein Expression and Purification: The bacterial host for protein expression was *E. coli* BL21 (DE3) carrying the desirable plasmid. The cells were grown in Luria broth (LB) with 0.1% antibiotic in baffled shaker flasks at 37 °C until mid-log phase (OD600 of ≈0.6–0.9), followed by induction of protein expression with 3 mM isopropyl β-D-1-thiogalactopyranoside (IPTG, Sangon Biotech) at 16 °C for 20 h with vigorous shaking (220 rpm). The S-A protein showed higher expression at 16 °C than at 37 °C, with a yield of 22.16 ± 6.90 mg per liter of cell culture ($n = 4$) after Ni-NTA purification, eluate purity>95%, and molecular weight of ≈35 kDa according to SDS-PAGE analysis (Figure 2; Figure S2, Supporting Information). The S-A spinning dope was prepared by concentrating the protein solution to ≈250 mg mL^{-1}, which became a viscous and transparent yellowish solution in Tris-buffered saline (TBS, pH 8.0) (Figure S3a, Supporting Information). The NTD2RCTD-SpyTag protein maintained high solubility and stability that allowed for storage at 4 °C in TBS (pH 8.0) or weeks (16). The expressions of AGFPA, BGFPB, BCFPB, BcpYFPB, BmCherryB, BSaTB, B2RGDB, and BLMB in *E. coli* were induced at 37 °C for 4 h.

The cells were harvested by centrifugation at 4200 × g, 4 °C for 40 min. Cell pellets were resuspended in buffer A (250 mM NaCl, 25 mM Tris-HCl, pH 8.0) and frozen at −80 °C overnight before protein purification. Phenylmethylsulfonyl fluoride (PMSF, 1 mM) was added to the suspension to inhibit serine protease, followed by sonication to lyse cells. Supernatants were collected by centrifugation at 28000 × g, 4°C for 60 min, and then loaded onto the HisTrap Ni-NTA affinity columns (Cytiva). The target protein was eluted by buffer B (250 mM NaCl, 25 mM Tris-HCl, 250 mM imidazole, pH 8.0). Protein purity was assessed using SDS-PAGE and Coomassie Brilliant Blue staining, with the Wide-Range True Color Two-Color Pre-Stained Protein Marker (Sangon Biotech) used as a size standard.

The purified S-A protein was concentrated to ≈250 mg mL^{-1} using Amicon Ultra centrifugal filters (Millipore) with a 10 kDa cutoff at 4000 × g, 4 °C. The protein concentration was determined by measuring the absorbance at 280 nm with a NanoDrop 2000 Spectrophotometer (Thermo Scientific) after diluting the solution 100 times in PBS. The highly concentrated protein solution was stored at 4 °C without agitation before spinning.

The purified proteins, including AGFPA, BGFPB, BCFPB, BcpYFPB, BmCherryB, and BSaTB, were buffer-exchanged against PBS using HiTrap desalting columns (Cytiva). The protein solutions were sub-packaged into 1.5 mL Eppendorf tubes, flash-frozen in liquid nitrogen, and stored in a −80 °C freezer.

The purified B2RGDB and BLMB proteins were dialyzed against Milli-Q water (4.5 L × 6) at 4 °C and centrifuged at 5200 × g for 30 min to remove precipitants. The resulting protein solutions were flash-frozen in liquid nitrogen and lyophilized with a FreeZone 4.5 Liter-105C Benchtop Freeze Dryer (Labconco) for five days. The lyophilized protein powders were stored at -80 °C before use.

Biomimetic Silk Spinning: A 1 mL syringe with a Luer Lok tip was filled with spinning dope and connected to a 34 G stainless steel blunt tip needle with an inner diameter of 0.06 mm. The concentrated spinning dope was extruded into an acidic coagulation bath at a smooth flow rate of 1.2 mL h^{-1} using a syringe pump (Pump 11 Pico Plus Elite, Harvard Apparatus). Silk threads were collected by a submerged roller and kept in the spinning buffer for at least 48 h before use. To test the influence of ions on silk, different buffer systems at pH 5 were used for coagulation, including 100 mM NaAc/HAc, 100 mM Na_3PO_4/H_3PO_4, and 500 mM NaAc/HAc with 250 mM KCl or NaCl.

Decoration of Spider Silk via Spy Chemistry: Spy spider silk fibers were washed sequentially with ddH_2O, PBS with 1% Triton X-100 (PBST), and ddH_2O. Spy chemistry was initiated by immersing the silk in the PBS solution of designated SpyCatcher-fusion protein (i.e., BGFPB, BCFPB, BcpYFPB, BmCherryB, or BSaTB, 1 mg mL^{-1}; B2RGDB and BLMB, 20 mg mL^{-1}). The resulting silk threads were washed again using ddH_2O, PBST, and ddH_2O to eliminate non-specific bindings.

Silicification on Spider Silk: Silicatein-laden spider silk fibers were immersed in a solution of 100 mM tetraethyl orthosilicate (TEOS) in PBS and incubated at 25 °C for 24 h with shaking at 150 rpm.[26d] After the incubation, the silk threads were washed with PBS and ddH_2O, and then dried in a sealed container containing silica gel beads for two days.

SEM and XPS Analyses of Recombinant Spider Silk: The silk morphology and size were examined using a JSM-6700F field emission scanning electron microscope (FE-SEM) with an acceleration voltage of 10.0 kV. The silk threads were coated with a thin gold layer using a Gold Sputter Coater (Quorum Q150T S). The micrographs were captured using a secondary electron detector. To determine the silk diameters, five spots were evaluated on each silk thread, with two independent silk samples analyzed.

To determine the Si chemical states on the silk surface, X-ray photoelectron spectra (XPS) were obtained using a PerkinElmer Physical Electronics 5600 spectrometer with a 400 μm X-ray beam from an Al Kα monochromatic source ($h\nu$ = 1486.6 eV). The detection angle of X-ray photoelectrons was set at 45° relative to the sample surface. The C 1s core level peak at 284.8 eV was used to calibrate the binding energy. The photoelectron peak areas were calculated using Shirley background correction in quantitative XPS analysis.[34] Peak fitting (Gauss-type profiles) was performed using the CasaXPS software (version 2.3.24 Pre-rel 1.0, CasaXPS Ltd., Teignmouth, United Kingdom).

Cell Cultures: To prepare the stainless-steel frames, wires with a thickness of 0.50 mm were manually bent into a square shape of ≈ 2 cm × 2 cm in size. The frames were then manually woven with silks in an even mesh pattern (Figure S8, Supporting Information). After weaving, the frames were rinsed with 70% ethanol and sterilized under UV light in a biosafety cabinet for 30 minutes.

For the cell culture experiments, human umbilical vein endothelial cells (HUVECs, Lonza) were cultured in Endothelial Microvasculature Growth Medium (EGM-MV BulletKit, Lonza). Cells up to passage 7 were used and grown to 70–80% confluency. The HUVECs were gently dripped onto the specimens placed in 60 mm cell culture dishes at a seeding density of 0.5×10^6 cells mL^{-1}. The initial incubation period for cell attachment lasted 24 h in a humidified incubator at 37 °C and 5% CO_2, with the medium being changed every two days.

Cell Attachment Assessment: The HUVECs attached to the silk surface were counted using phase-contrast images captured by a Nikon C2+ Laser Scanning Confocal Microscope on days 1, 3, 6, and 8. The number of cells per unit millimeter was determined using ImageJ (NIH) with the cell counter plug-in.

Cell Viability and Proliferation Assessment: The proliferation of HUVECs on silk fibers was assessed by collecting images of LIVE/DEAD Cell Imaging Kit (Invitrogen)-stained cells on days 6, 10, and 13, according to the manufacturer's guidelines. The stained cells were visualized using a Nikon C2+ Laser Scanning Confocal Microscope. Fluorescence and Z-stack scanning images were collected using NIS-Elements AR software.

Viability, area coverage, and aspect ratio of cells were analysed using ImageJ. The percentage of viable cells was determined using the equations below:

$$\text{Cell viability} = \frac{\text{Live cell number}}{\text{Total cell number}} \times 100\% \quad (1)$$

The area coverage of cells was determined based on the equation below:

$$\text{Area coverage of cells} = \frac{\text{Total area of cells}}{\text{Surface area of silk}} \times 100\% \quad (2)$$

The aspect ratio, calculated as below, was used to quantify the propensity of HUVECs to form networks.[35] The aspect ratio was defined as the ratio of cell length to width.

$$\text{Aspect ratio} = \frac{\text{Cell length}}{\text{Cell width}} \quad (3)$$

Statistical significance was assessed using two-way Analysis of Variance (ANOVA) in GraphPad Prism 9. Four independent experiments were performed.

Supporting Information

Supporting Information is available from the Wiley Online Library or from the author.

Acknowledgements

This work was supported by Ministry of Science and Technology 2020YFA0908100 (F.S.); Natural Science Foundation of China Excellent Young Scientists Fund NSFC21EG08 (F.S.); Guangdong Natural Science Foundation GDST19EG22 (F.S.); Research Institute of Tsinghua, Pearl River Delta #RITPRD21EG01 (F.S.); Science, Technology and Innovation Commission of Shenzhen Municipality Basic Research Program Grant #JCYJ20190813094601656 (F.S.) and Key Research Program Grant #JCYJ20200109141241950 (F.S.); and Research Grants Council of Hong Kong SAR GRF Grant #16103519 and #16103421 (F.S.) and #26101016, #16101118, #16101918, #C6002-17G, #GC6018-19G, #16209820 (A.R.W); Hong Kong University of Science and Technology's startup grant no. R9364 and the Lo Ka Chung Foundation through the Hong Kong Epigenomics Project and the Chau Hoi Shuen Foundation (A.R.W.); Hong Kong PhD Fellowship Scheme (Sin Yen Tan). XPS service: Materials Characterization & Preparation Facility (MCPF), HKUST; MALDI-TOF service: Biosciences Central Research Facility (BioCRF), HKUST; The authors gratefully acknowledge the valuable technical support provided by Xudong Peng on the scanning electron microscope.

Conflict of Interest

F.S. and B.J. are inventors on a patent application (FI-221631-5952) filed through the Hong Kong University of Science and Technology.

Author Contributions

B.J., S.T., and S.F. contributed equally to this work. F.S. and B.J. conceived the idea. B.J. and S.T. designed the project and experiments. B.J., S.T., S.F., X.F., and H.K.F.F. conducted the experiments. B.M.P., Z.Y. R.W., and S.K. contributed to the data analysis and discussion. F.S., A.R.W., B.J., and S.T. analyzed data and wrote the manuscript. All authors reviewed the final manuscript and provided inputs.

Data Availability Statement

The data that support the findings of this study are available in the supplementary material of this article.

Keywords

biomaterials, cell adhesion, click chemistry, silicification, spider silk

Received: April 14, 2023
Revised: May 27, 2023
Published online:

[1] a) F. Schäfer-Nolte, K. Hennecke, K. Reimers, R. Schnabel, C. Allmeling, P. M. Vogt, J. W. Kuhbier, U. Mirastschijski, *Ann. Surg.* **2014**, *259*, 781; b) J. W. Kuhbier, K. Reimers, C. Kasper, C. Allmeling, A. Hillmer, B. Menger, P. M. Vogt, C. Radtke, *J. Biomed. Mater. Res., Part B* **2011**, *97*, 381.

[2] a) Z. Liu, W. Liu, C. Hu, Y. Zhang, X. Yang, J. Zhang, J. Yang, L. Yuan, *Opt. Express* **2019**, *27*, 21946; b) H. Venkatesan, J. Chen, H. Liu, Y. Kim, S. Na, W. Liu, J. Hu, *Mater. Chem. Front.* **2019**, *3*, 2472; c) Z. Liu, M. Zhang, Y. Zhang, Y. Zhang, K. Liu, J. Zhang, J. Yang, L. Yuan, *Opt. Lett.* **2019**, *44*, 2907.

[3] a) A. R. Franco, E. M. Fernandes, M. T. Rodrigues, F. J. Rodrigues, M. E. Gomes, I. B. Leonor, D. L. Kaplan, R. L. Reis, *Acta Biomater.* **2019**, *99*, 236; b) K. Hennecke, J. Redeker, J. W. Kuhbier, S. Strauss, C. Allmeling, C. Kasper, K. Reimers, P. M. Vogt, *PLoS One* **2013**, *8*, e61100.

[4] S. Kubik, *Angew. Chem., Int. Ed.* **2002**, *41*, 2721.

[5] a) N. Huby, V. Vié, A. Renault, S. Beaufils, T. Lefevre, F. Paquet-Mercier, M. Pézolet, B. Bêche, *Appl. Phys. Lett.* **2013**, *102*, 123702; b) A. Kiseleva, G. Kiselev, V. Kessler, G. Seisenbaeva, D. Gets, V. Rumyantseva, T. Lyalina, A. Fakhardo, P. Krivoshapkin, E. Krivoshapkina, *ACS Appl. Mater. Interfaces* **2019**, *11*, 22962.

[6] a) A. Resch, S. Wolf, A. Mann, T. Weiss, A.-L. Stetco, C. Radtke, *Int. J. Mol. Sci.* **2018**, *20*, 71; b) T. Kornfeld, P. M. Vogt, V. Bucan, C.-T. Peck, K. Reimers, C. Radtke, *J Funct Biomater* **2016**, *7*, 30; c) C. Radtke, *Int. J. Mol. Sci.* **2016**, *17*, 1754; d) F. Millesi, T. Weiss, A. Mann, M. Haertinger, L. Semmler, P. Supper, D. Pils, A. Naghilou, C. Radtke, *FASEB J.* **2021**, *35*, e21196.

[7] K. Schacht, T. Scheibel, *Curr. Opin. Biotechnol.* **2014**, *29*, 62.
[8] M. Andersson, Q. Jia, A. Abella, X.-Y. Lee, M. Landreh, P. Purhonen, H. Hebert, M. Tenje, C. V. Robinson, Q. Meng, *Nat. Chem. Biol.* **2017**, *13*, 262.
[9] A. Rising, J. Johansson, *Nat. Chem. Biol.* **2015**, *11*, 309.
[10] M. Widhe, J. Johansson, M. Hedhammar, A. Rising, *Biopolymers* **2012**, *97*, 468.
[11] a) F. Sun, W.-B. Zhang, *Chin. Chem. Lett.* **2017**, *28*, 2078; b) F. Sun, W. B. Zhang, *Chin. J. Chem.* **2020**, *38*, 894.
[12] F. Sun, W.-B. Zhang, A. Mahdavi, F. H. Arnold, D. A. Tirrell, *Proc. Natl. Acad. Sci. USA* **2014**, *111*, 11269.
[13] J. Jeon, S. V. Subramani, K. Z. Lee, B. Jiang, F. Zhang, *Int. J. Mol. Sci.* **2023**, *24*, 6416.
[14] a) F. Hagn, L. Eisoldt, J. G. Hardy, C. Vendrely, M. Coles, T. Scheibel, H. Kessler, *Nature* **2010**, *465*, 239; b) C. Rat, J. C. Heiby, J. P. Bunz, H. Neuweiler, *Nat. Commun.* **2018**, *9*, 4779.
[15] a) N. Kronqvist, M. Otikovs, V. Chmyrov, G. Chen, M. Andersson, K. Nordling, M. Landreh, M. Sarr, H. Jörnvall, S. Wennmalm, *Nat. Commun.* **2014**, *5*, 3254; b) N. A. Oktaviani, A. Matsugami, A. D. Malay, F. Hayashi, D. L. Kaplan, K. Numata, *Nat. Commun.* **2018**, *9*, 2121; c) M. Sarr, K. Kitoka, K.-A. Walsh-White, M. Kaldmäe, R. Metlāns, K. Tārs, A. Mantese, D. Shah, M. Landreh, A. Rising, *J. Biol. Chem.* **2022**, *298*, 101913.
[16] a) M. Landreh, G. Askarieh, K. Nordling, M. Hedhammar, A. Rising, C. Casals, J. Astorga-Wells, G. Alvelius, S. D. Knight, J. Johansson, *J. Mol. Biol.* **2010**, *404*, 328; b) M. Andersson, G. Chen, M. Otikovs, M. Landreh, K. Nordling, N. Kronqvist, P. Westermark, H. Jörnvall, S. Knight, Y. Ridderstråle, *PLoS Biol.* **2014**, *12*, e1001921.
[17] S. Pahari, L. Sun, E. Alexov, *Database* **2019**, 2019.
[18] R. Evans, M. O'Neill, A. Pritzel, N. Antropova, A. Senior, T. Green, A. Žídek, R. Bates, S. Blackwell, J. Yim, *bioRxiv* **2021**, 2021.10.04.463034.
[19] M. Mirdita, K. Schütze, Y. Moriwaki, L. Heo, S. Ovchinnikov, M. Steinegger, *Nat. Methods* **2022**, *19*, 679.
[20] a) M. N. Tahir, P. Théato, W. E. Müller, H. C. Schröder, A. Janshoff, J. Zhang, J. Huth, W. Tremel, *Chem. Commun.* **2004**, 2848; b) T. Elkhooly, W. Müller, X. Wang, W. Tremel, S. Isbert, M. Wiens, *Bioinspiration Biomimetics* **2014**, *9*, 044001; c) M. Wiens, T. A. Elkhooly, H.-C. Schröder, T. H. Mohamed, W. E. Müller, *Acta Biomater.* **2014**, *10*, 4456; d) K. Shimizu, D. E. Morse, *Methods in Enzymology*, Vol. *605*, Elsevier, Amsterdam **2018**, p. 429; e) H. Schroder, V. Grebenjuk, X. Wang, W. Müller, *Bioinspir. Biomim.* **2016**, *11*, 041002.
[21] a) M. T. Conconi, F. Ghezzo, M. Dettin, L. Urbani, C. Grandi, D. Guidolin, B. Nico, C. Di Bello, D. Ribatti, P. P. Parnigotto, *J. Pept. Sci.* **2010**, *16*, 349; b) R. Cruz-Acuña, M. Quirós, S. Huang, D. Siuda, J. R. Spence, A. Nusrat, A. J. García, *Nat. Protoc.* **2018**, *13*, 2102; c) J. Jia, E. J. Jeon, M. Li, D. J. Richards, S. Lee, Y. Jung, R. W. Barrs, R. Coyle, X. Li, J. C. Chou, *Sci. Adv.* **2020**, *6*, eaaz5894; d) D. Diana, B. Ziaco, G. Colombo, G. Scarabelli, A. Romanelli, C. Pedone, R. Fattorusso, L. D. D'Andrea, *Chemistry* **2008**, *14*, 4164.
[22] D. P. Knight, F. Vollrath, *Naturwissenschaften* **2001**, *88*, 179.
[23] A. D. Malay, T. Suzuki, T. Katashima, N. Kono, K. Arakawa, K. Numata, *Sci. Adv.* **2020**, *6*, eabb6030.
[24] G. Askarieh, M. Hedhammar, K. Nordling, A. Saenz, C. Casals, A. Rising, J. Johansson, S. D. Knight, *Nature* **2010**, *465*, 236.
[25] G. Greco, J. Francis, T. Arndt, B. Schmuck, F. G. Bäcklund, A. Barth, J. Johansson, N. M. Pugno, A. Rising, *Molecules* **2020**, *25*, 3248.
[26] a) W. E. Müller, A. Krasko, G. L. Pennec, R. Steffen, M. Wiens, M. S. A. Ammar, I. M. Müller, H. C. Schröder, *Silicon Biomineralization: Biology—Biochemistry—Molecular Biology—Biotechnology*, Springer, Berlin **2003**, p. 195; b) K. Shimizu, J. Cha, G. D. Stucky, D. E. Morse, *Proc. Natl. Acad. Sci. USA* **1998**, *95*, 6234; c) Y. Zhou, K. Shimizu, J. N. Cha, G. D. Stucky, D. E. Morse, *Angew. Chem., Int. Ed.* **1999**, *38*, 779; d) J. N. Cha, K. Shimizu, Y. Zhou, S. C. Christiansen, B. F. Chmelka, G. D. Stucky, D. E. Morse, *Proc. Natl. Acad. Sci. USA* **1999**, *96*, 361.
[27] J. W. Kuhbier, C. Allmeling, K. Reimers, A. Hillmer, C. Kasper, B. Menger, G. Brandes, M. Guggenheim, P. M. Vogt, *PLoS One* **2010**, *5*, e12032.
[28] a) S. Sagnella, F. Kligman, R. E. Marchant, K. Kottke-Marchant, *J. Biomed. Mat. Res.* **2003**, *67*, 689; b) V. Marchi-Artzner, B. Lorz, U. Hellerer, M. Kantlehner, H. Kessler, E. Sackmann, *Chemistry* **2001**, *7*, 1095.
[29] a) G. E. Davis, D. R. Senger, *Circ. Res.* **2005**, *97*, 1093; b) V. Iorio, L. D. Troughton, K. J. Hamill, *Adv Wound Care* **2015**, *4*, 250.
[30] R. Mazor, T. Alsaigh, H. Shaked, A. E. Altshuler, E. S. Pocock, E. B. Kistler, M. Karin, G. W. Schmid-Schönbein, *J. Biol. Chem.* **2013**, *288*, 598.
[31] M. Pierschbacher, E. G. Hayman, E. Ruoslahti, *Proc. Natl. Acad. Sci. USA* **1983**, *80*, 1224.
[32] B. Turk, L. Huang, E. Piro, L. Cantley, *Nat Biotechnol* **2001**, *19*, 661.
[33] H. Nagase, G. B. Fields, *Biopolymers* **1996**, *40*, 399.
[34] D. A. Shirley, *Phys. Rev. B* **1972**, *5*, 4709.
[35] R. L. Saunders, D. A. Hammer, *Cell Mol. Bioeng.* **2010**, *3*, 60.